Random Vibration Simulation and Testing of a Compact, Magnetic Bearing Supported Blower for Space Applications

Larry Hawkins[1], Rasish Khatri[1], Alexei Filatov[1]
Chris DellaCorte[2], and S. Adam Howard[2]
[1]Calnetix Technologies, Cerritos, CA, USA
[2]NASA Glenn Research Center, Cleveland, OH, USA
lhawkins@calnetix.com

Abstract

NASA is developing a next-generation CO_2 removal system, the Four Bed Carbon Dioxide Scrubber (4BCO2), which will use the International Space Station (ISS) as a testbed. A key component of both the existing and the new system is the blower that provides the airflow through the CO_2 sorbent beds. To improve performance and reliability, magnetic bearings will be used in lieu of more conventional bearings (e.g. ball bearings or hydrodynamic bearings) to improve resistance to contaminants and enable extensibility with regards to blower speed, pressure rise and mass flow rate. The new blower features a high-efficiency permanent magnet motor, a five-axis, active magnetic bearing system, and a compact controller containing both a variable speed drive and magnetic bearing controller. The blower uses a centrifugal impeller to pull air from the inlet port and drive it through an annular space around the motor and magnetic bearing components to the exhaust port. Technical challenges of the blower and controller development include survival of the blower system under launch random vibration loads, operation in microgravity, packaging under strict size and weight requirements, and successful operation during 4BCO2 operational changeovers. Each serial build of the blower must pass a severe random vibration test to prove it will survive launch conditions. This paper discusses the vibration test requirements and provides details of a simulation performed to estimate the peak backup bearing displacements and loads. Results from the successful random vibration testing of the prototype build are discussed and compared to the simulation.

Introduction

A new magnetically-levitated blower was recently developed for use in a new 4BCO2 to be tested on the ISS. The blower, shown in Figure 1, features a high-efficiency permanent magnet motor, a five-axis, active magnetic bearing system, and a compact controller containing both a variable speed drive and magnetic bearing controller. Design considerations for the blower system active magnetic bearings (AMB) and backup bearings were previously discussed in detail [1], including magnetic finite element analysis (FEA) of the actuator/sensor system, rotordynamics/controls analysis, and backup bearing drop simulations. The design is briefly reviewed here to provide background to the reader.

All equipment that is delivered to the ISS is exposed to a significant level of launch vibration which is characteristically random in nature. NASA requires such equipment to pass a random vibration proof test to ensure it can survive the flight environment. The vibration level and frequency spectrum depend on the nature of the equipment and how it is packaged. Although the blower will be launched under soft-stow conditions, the low frequency vibration environment is still quite severe. The blower and controller will be deactivated during the launch so the magnetic bearings will be de-levitated which for standard AMB applications means the rotor is supported on the backup bearings rather than the magnetic bearings. However, due to the high imposed vibration level during the launch, consideration was given to using a locking mechanism (launch locks) to keep the rotor from bouncing in the backup bearing clearance space and potentially causing impact damage to the backup bearings. Several analysis steps were undertaken to assess the need for launch locks and to evaluate potential locking strategies. This included a transient simulation using a forcing function derived from the NASA specified Power Spectral Density (PSD) random vibration level. The simulation methodology and results are discussed here along with test results from the shaker table testing of the blower. The Magnetic Bearing Controller (MBC) was activated during the vibration testing to allow collection of rotor/housing relative displacement test data from the AMB position sensors. This data is discussed and compared to the simulation results.

Blower Design

The design of the blower, magnetic bearings and backup bearings is discussed in detail by Hawkins [1] but is described here in limited detail for easy reference. Figure 1 shows the overall layout of the blower. The centrifugal impeller at the inlet (right side of the figure) draws in cabin air and pushes it through an annular passage to the outlet. This primary flow (blue arrows) provides cooling for the motor stator as it passes through axial slots in the laminated stator. A secondary flow (orange arrows) cools the bearing elements in the central part of the machine as well as the motor end turns near the outlet. The blower is designed to be operated at any speed from rest up to 60,000 rpm.

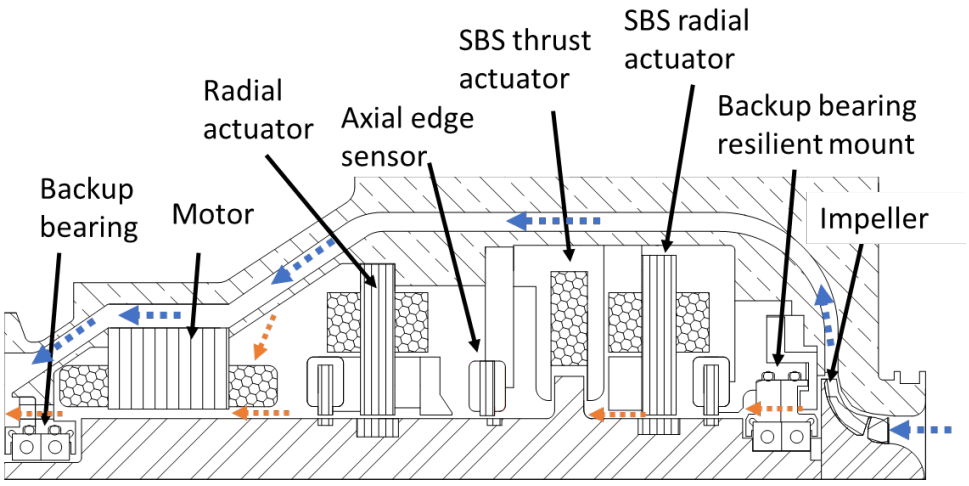

Figure 1. Layout of blower for the new 4BCO2 system (from Figure 2 of [1]).

The homopolar, permanent magnet (PM) biased magnetic bearings consist of a three-axis combination radial/thrust active magnetic bearing on the impeller side and a two-axis radial active magnetic bearing on the motor side. The basic design parameters for the magnetic bearings are summarized in Table 1. The radial position sensors are located just outboard of the actuators and the axial position sensor is between the two magnetic bearing sets. The backup bearings are comprised of resiliently mounted, angular contact ball bearings. The backup bearings serve to support the shaft when the magnetic bearings are de-activated, in the case of overload, or in the case of a critical component failure.

This new magnetic bearing blower is designed to replace a heritage foil bearing supported blower and must fit into the same length, width, and height envelope of 7.6 x 5 x 8 inches (193 x 127 x 203 mm). Additionally, the new blower was required to adapt to the inlet and outlet interface flanges of the existing system, 1.5 inch (38 mm) and 2.75 inch (70 mm) respectively. The overall design layout followed naturally from the need to meet the existing envelope and interface dimensions.

Table 1. Magnetic Bearing Design Parameters

Parameter	**Radial, Brg 1**	**Radial, Brg 2**	**Axial**
Minimal load capacity, N (lbf)	44 (10)	44 (10)	89 (20)
Force constant, N/A (lbf/A)	18.5 (4.17)	18.9 (4.25)	38.3 (8.61)
Negative stiffness, N/mm (lbf/in)	173 (990)	89 (510)	70 (400)
Magnetic air gap, mm (mil)	0.76 (30)	0.76 (30)	0.76 (30)
Slew corner frequency, Hz	1250	1250	282

Rotordynamic Structural Model

The rotordynamic structural model of the blower, rotor, and housing are shown in Figure 2. The rotor stiffness is modelled with Timoshenko beam elements with mass for each beam lumped at the nodes. The impeller is modelled as a lumped inertia at its center-of-gravity. The magnetic bearing and sensor laminations are assumed to contribute mass but no lateral stiffness due to the flexibility of the lamination bonding. The lateral stiffness contribution of the motor permanent magnets is derated, consistent with the authors' experience for this type of rotor construction. The springs to ground in the figure show the PM negative stiffness locations for the motor and magnetic bearings. The predicted AMB negative stiffnesses are in Table 1; the motor negative stiffness of 7.4 N/mm (42 lbf/in) is negligible by comparison but has been included for completeness.

The first forward free/free bending mode of the rotor is predicted to be at 139,200 cpm (2.3 kHz) at 0 rpm and 143,300 (2.4 kHz) at 60,000. The large critical speed margin and small gyroscopic effect allow for a relatively simple magnetic bearing control design for this machine. As rotor launch locks are to be investigated below, it is also important to consider the lowest natural frequency and corresponding mode shape of the rotor for several potential end conditions. Figure 3 shows two cases, a) rotor pinned to the housing at both ends, and b) the rotor connected to the housing with 40,000 lbf/in at the motor (left) end and the rotor pinned to the housing at the impeller (right) end. For the case of the rotor pinned on both ends, the lowest natural frequency is 37,370 cpm (620 Hz). For the second case the lowest natural frequency is 31,900 cpm (530 Hz).

Backup Bearing System

All active magnetic bearing systems include a backup (touch-down) bearing system to support the rotor during non-operation, overload of the AMBs, or component failure. A few specifications exist (or are being developed) that provide guidance on how to select and/or evaluate backup bearings (e.g. [2, 3]), but the practical process of backup bearing selection remains heavily experience and test driven within the AMB community. Schweitzer et. al [4] provides a bird's eye view of basic principles behind backup bearing modeling, selection, and analysis. Wilkes [5] provides perhaps the most comprehensive nonlinear backup bearing dynamic model to date.

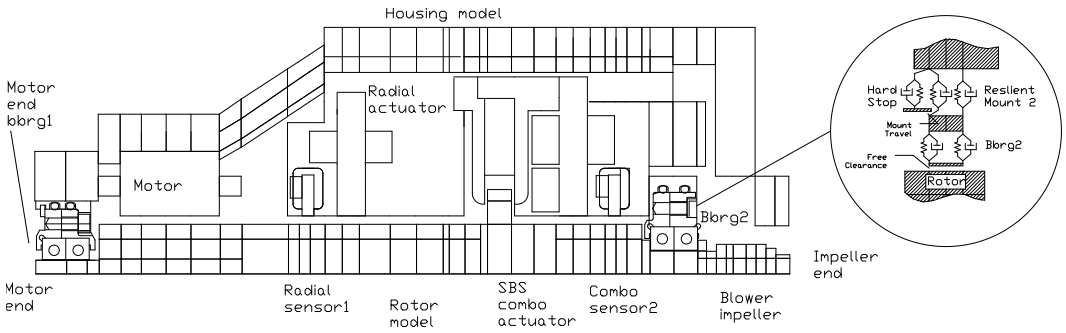

Figure 2. Geometry of the rotordynamic structural model of the blower.

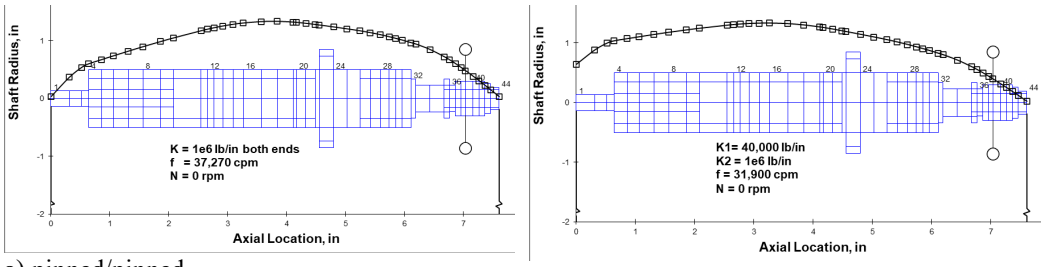

a) pinned/pinned b) shimmed/pinned

Figure 3. Lowest 0 rpm mode shape and natural frequency with a) rotor pinned at ends, b) 40,000 klb/in at motor end (left side) and pinned at impeller end (right side).

The backup bearings chosen for this blower are cageless, angular contact, duplex pairs with steel races and ceramic balls. The motor end (radial only) backup bearing assembly is shown in Figure 4. The bearing mount is resiliently supported by elastomer O-rings that provide impact compliance, damping and reduce whirl frequency during normal backup bearing operation. The impeller end, radial/thrust (combination) backup bearing assembly uses larger bearings and includes rotor mounted thrust surfaces but is otherwise similar to the motor end. The speed factors, nd_m, of the backup bearings are 0.81E6 and 1.08E6 mm-rpm at 60,000 rpm, where n is the speed in rpm and d_m is the average of the inside and outside diameter. The speed factors are lower than usual for backup bearings, making the design very robust thermally. This compact design was possible due to the relatively low speed, 60,000 rpm, for the size of the rotating assembly. The compactness of the design was a key factor in meeting the size constraint for the new blower.

Transient, nonlinear drop simulations discussed in [1] showed that the backup bearing design should perform well in response to operating overloads and/or drop transient and spin down situation. The same simulation tool is used here to investigate the response of the system and backup bearing loads due to launch vibrations. For the launch vibration simulation discussed below, the backup bearing system is modelled as shown in the inset on the right side of Figure 2. There is a free clearance between the inner rings of the bearings and the rotor landing surfaces such that they are not normally in contact. The radial and axial free clearances are ±0.114 mm (±0.0045 in) and ±0.127 mm (±0.005 in). Each backup bearing pair is supported in a resilient mount to limit peak impact loads during the rotor drop transient. The resilient mount will also reduce impact loads in case of rotor contact due to launch vibration. Clearances and relative stiffness values for the backup bearings and resilient mount are given in Table 2. The backup bearing stiffnesses are the ball/race stiffnesses provided by the bearing manufacturer. The stiffness and damping of the resilient mounts were estimated by scaling empirical data from [6].

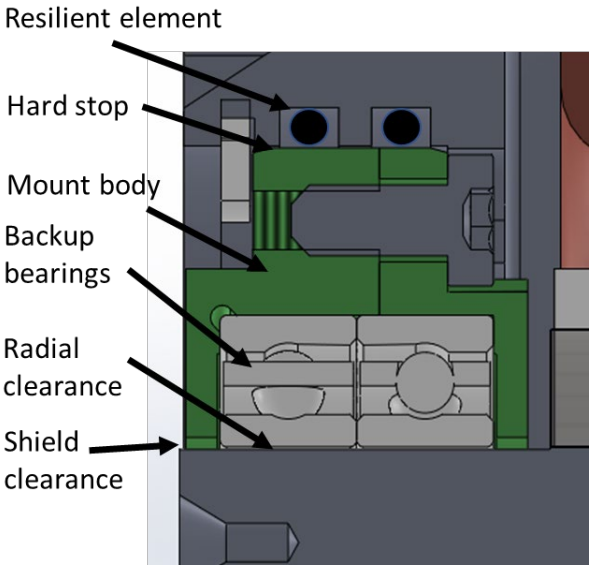

Figure 4. Radial end backup bearing assembly.

Table 2. Backup Bearing And Mount Characteristics

Parameter	Motor End (radial)	Impeller End (radial)	Impeller End (axial)
Free Clearance, mm (in)	0.114 (0.0045)	0.114 (0.0045)	0.127 (0.005)
Resilient Mount Travel, mm (in)	0.076 (0.003)	0.076 (0.003)	0.051 (0.002)
Backup Bearing Stiff (pair), N/mm (lbf/in)	22,800 (130,000)	43,800 (250,000)	9,600 (55,000)
Resilient Mount Stiffness N/mm (lbf/in)	900 (5,200)	1,100 (6,000)	--
Radial Hard Stop Stiffness, N/mm (lbf/in)	114,000 (650,000)	220,000 (1,250,000)	48,000 (275,000)

Random Vibration Requirements

NASA imposes random vibration requirements for payloads that consist of electronic equipment sent to the ISS (International Space Station) [7]. The goal is to ensure the appropriate random vibration proof test has been performed and that the item can survive the flight environment. The blower and controller will be sent as a "soft stowed" payload meaning they are not hard mounted to the launch vehicle structure. The required protoflight vibration testing requirements for this are shown in Table 3 and Figure 5. The protoflight test level is constructed from two parts: 1) the envelope of the maximum expected flight level (MEFL) + 3db margin, and 2) the minimum workmanship level (MWL). The MEFL is the maximum vibration expected during launch, including the soft-stow packaging effects. The vibration level of 0.35 G^2/Hz from 20 – 100 Hz with roll-off at 15 dB per decade at higher frequencies comes from this launch requirement. This is the portion of the curve that is of most concern for the blower and in assessing the design of the launch locks for the backup bearings. The MWL, 0.04 G^2/Hz up to 500 Hz with roll-off at 3 dB per decade at higher frequencies is an environmental stress screen and provides confidence in the assembly process and screens for latent defects.

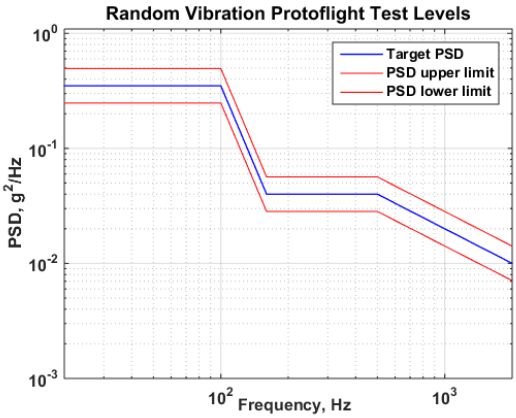

Figure 5. Random vibration protoflight test spectrum for the blower system.

Table 3. Random Vibration Protoflight Test Level

Frequency (Hz)	**Protoflight Test Level (g^2/Hz)**
20	0.35
100	0.35
100 - 160	-15.4 dB/octave slope
160 - 500	0.04
500-2000	-3 dB/octave slope
2000	0.01
Overall	8.8 g_{rms}
Duration	1 min/axis

Launch Locks

As the blower will be launched to the ISS with the magnetic bearings deactivated, the backup bearings could provide support of the rotor during launch. An alternative is to use launch locks to limit rotor motion and backup bearing contact during the launch. Due to the need for a compact design, design priority was given to ensuring the backup bearings were robust to typical backup bearing service such as a drop transient and spin down. It was expected at the outset that launch locks might be needed to limit the peak backup bearing loads during launch. A time simulation using the vibration level of Figure 5 was performed to evaluate the options. Several strategies were considered:

Case 1: No launch locks – rely on the magnetic bearing PM bias passive negative stiffness force of 5 lbf radially at the two backup bearing locations and 6 lbf axially to mitigate rotor motion.

Case 2: Axial/radial pinning – pin the rotor at the ends such that the rotor is held in the center of the backup bearing clearance spaces both radially and axially.

Case 3: Axial/combo radial pin, radial end shim – use a shim to take up the clearance space in the motor end backup bearing with the rotor in the center of the radial/axial clearance space on the thrust end.

Figure 6 shows a cross-section of the machine with the basic launch lock concept in place. A key requirement was that the launch locks be easy to remove, and once removed, the blower could be installed in the 4BCO2 system with no reassembly or adjustments. As such, the impeller end lock attaches with captive screws to the impeller housing. The motor end lock is attached with the

same V-band clamp used to connect the blower to the 4BCO2 ducting. In the axial direction, there is an adjustment screw to clamp the rotor axially against a stiff spring. During a one-time shop set up process, the rotor radial positions can reliably be set to the backup bearing center (or to the side) using the magnetic bearing position sensors for reference. However, there is some concern that the V-band clamp is not precise enough to locate the rotor in the desired position if it is removed and reattached. For this reason, an alternate option (Case 3 above) was created to shim the motor end backup bearing to take up the free clearance space between the rotor journal and backup bearing inner ring. This is possible because the motor end backup bearing clearance space is accessible with the machine assembled. The planned vibration testing was simulated to evaluate the three cases above. A review of the simulation approach and results are described below.

An important criterion for evaluating the launch locks is the peak transient load allowed. The goal was to keep the peak impact loads below 95 lbf (420 N) for the motor end backup bearings and below 200 lbf (890 N) for the impeller end backup bearings. The peak predicted loads for the previously reported drop simulation and spin down were 18 lbf (80 N) and 39 lbf (175 N) for the motor end and impeller end backup bearings, respectively.

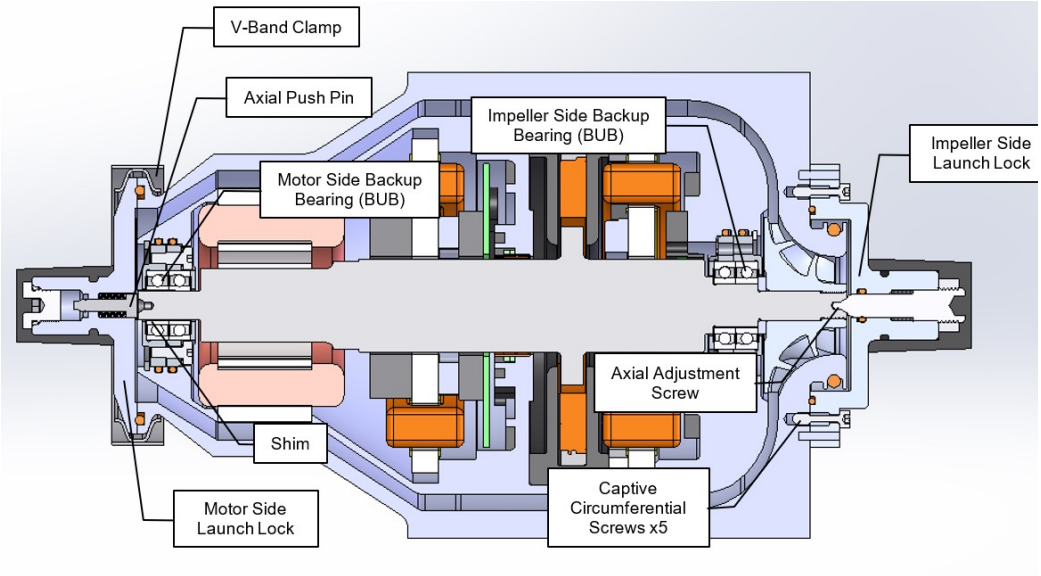

Figure 6. Blower cross-section showing launch locks.

Random Vibration Simulation

Each lock strategy was examined by using a transient, nonlinear simulation tool that is often used for rotor drop transient analysis. To drive the simulation, a forcing function time history was synthesized that would produce a base motion meeting the required PSD of Figure 5. It should be noted that there are many possible time histories that would meet the PSD specification as the relative phases are random. In general, a truly random vibration signal will contain all frequencies in the frequency band of interest and the amplitudes and phases of each frequency will vary randomly. However, the average amplitudes tend to remain relatively constant for many processes and the PSD is used to provide a statistical characterization of this.

During testing, the housing will be firmly clamped to the shaker table and is expected that the housing motion at the supports will follow the prescribed acceleration of the shaker table. It is convenient in the simulation tool to apply a driving force to the model support degrees-of-freedom that produces the prescribed acceleration. By using soft supports in the simulation model, with housing rigid body natural frequencies well below the low end of the vibration spectrum (20 Hz), the necessary driving force, f_{Sx}, can be calculated from:

$$f_{S,x} = m_{cas}\, \ddot{x}_{cas} \qquad (1)$$

where m_{cas} is the mass of the housing in the simulation model, and $\ddot{x}_{cas}$ is an acceleration time history derived from the required PSD. The simulation approach used here is very similar to the one described in detail by Hawkins [8] to model shock impact into the housing support of a magnetic bearing supported compressor.

There are several ways to synthesize a time history from a PSD. The approach used here is to follow these steps:

1) Generate a series of sine waves with random phases and with frequencies, $f_{exc,i}$, ranging from 20 Hz to 2000 Hz, separated by delta frequency, df_{exc}, of 0.5 Hz.
2) Scale the sine waves per the PSD requirement. If the required acceleration level in $Grms^2/Hz$ at frequency, $f_{exc,i}$, is ASD_i, then the amplitude of the sine wave at that frequency, X_i, is:

$$X_i = \sqrt{2\, df_{exc}\, ASD_i}$$

where the factor $\sqrt{2}$ is the conversion form RMS to peak for an individual sine.

3) Sum the sine waves point by point to get the pseudo random input time history.
4) Perform a Fourier transform and scaled to PSD to verify the synthesized time history matches the required spectrum.

The resulting time history, shown in Figure7, is not unique as phase is not part of the PSD. The time history is expected to follow a normal distribution as verified by the histogram in Figure 8. To verify that the generated time history in Figure 7 meets the requirements, its power spectrum is calculated using the built-in Matlab function *pwelch.m*. The result is shown in Figure 9 verifies good compliance with the specification except for a few excursions at higher frequencies where the PSD amplitude is lower. Another method, not used here, to generate the required time history is to start with a purely random (white noise) time history and take a Fourier transform to get spectral components, then scale these components starting at Step 2 above.

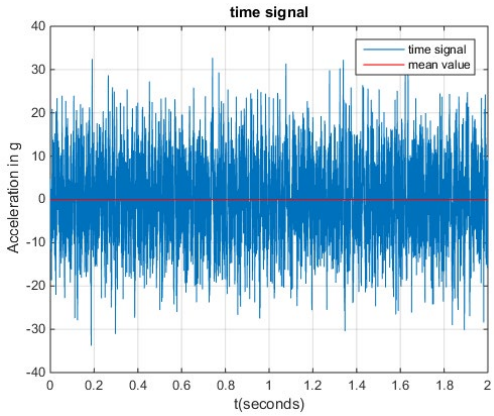

Figure 7. Accel time history synthesized to meet protoflight test level PSD.

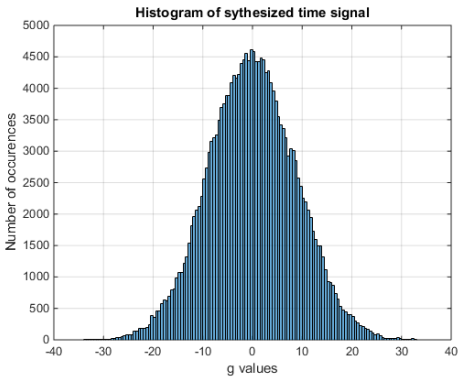

Figure 8. Histogram of synthesized random vibration time history.

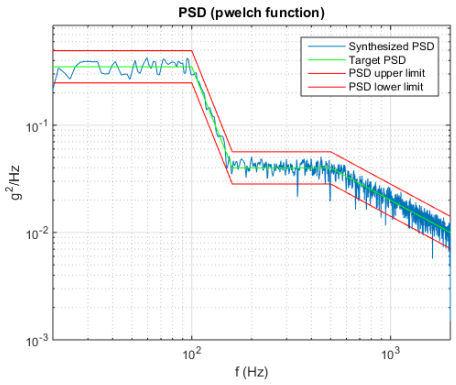

Figure 9. PSD of synthesized time history, from Matlab pwelch.m for confirmation.

Simulation Results

Figures 10-15 show simulation results for the three cases described above: Case 1: no launch locks, Case 2: axial/radial pinning, and Case 3: radial end shim, axial/combo radial pin. For each case, initial conditions were used that place the rotor in a neutral position. This was accomplished by running an initial simulation with no external excitation and using the final conditions from that run as the initial conditions for the simulation run with excitation. The rotor spin axis was horizontal for all tests (discussed below), so the same was assumed for the simulations. Simulation results are shown for vertical excitation for brevity. The horizontal excitation results differ only by the direction of the gravity vector relative to the excitation. Case 1 displacement trajectories with horizontal excitation differed from the vertical excitation but the number of excursions past 50% of design limit load were similar.

Figure 10-11 show predicted behavior for Case 1, no launch locks. Figure 10 shows relative rotor/backup bearing displacement. At start the rotor rests on the backup bearings, 0.0045 in from center as that minimum clearance was used for the simulations. Figure 10 shows many excursions where the rotor pulls out of contact with the backup bearing, crossing into the clearance space in response to the imposed motion. Figure 11 shows backup bearing loading during the simulation. The initial load of ~5 lbf at start is due to gravity and the PM negative stiffness offset force pulling the rotor against the backup bearings. For the smaller, motor end backup bearing there are ten load excursions above 47.5 lbf (half of the 95 lbf design limit). For the larger, impeller end backup bearing there are five load excursions above 100 lbf (half of the 200 lbf design limit).

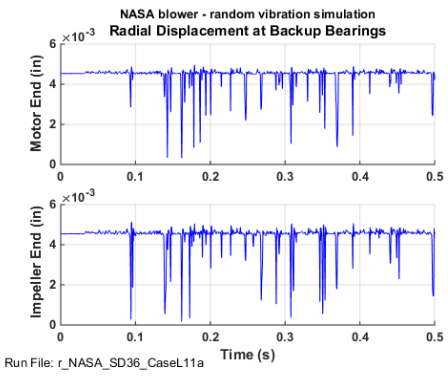

Figure 10. Predicted relative rotor/backup bearing displacement magnitudes. Case1: no launch locks.

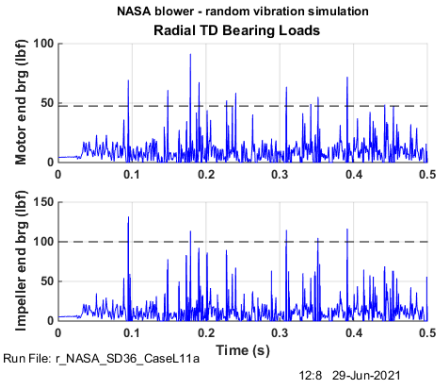

Figure 11. Predicted backup bearing loads. Case1: no launch locks.

Figure 12 shows predicted behavior for Case 2, rotor pinned at each end to the housing. This was accomplished by connecting a discrete 1e6 lbf/in stiffness between rotor end degrees-of-freedom and the corresponding housing degrees-of-freedom. Figure 10 shows relative rotor/backup bearing displacement. The peak excursion is 0.0001 in at the motor end bearing and 0.0035 in at the impeller end bearing. The impeller end bearing displacement is further from the shaft end where the rotor is pinned so the excursion should be higher. The dominant response frequency is at 690 Hz which can be compared to the prediction of 620 Hz for first pinned/pinned mode. The rotor does not contact the backup bearing so there is no load plot to show. This is the desired result, but as mentioned above, there is concern about reliably fixing the rotor at the backup bearing center on the motor end.

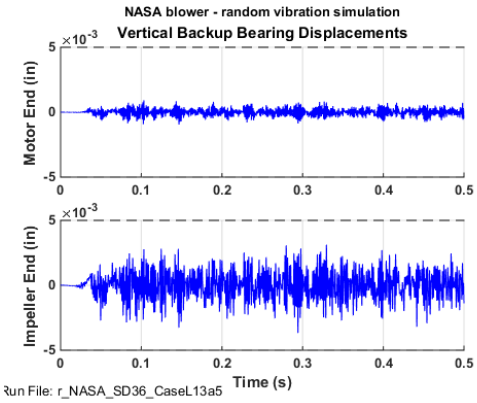

Figure 12. Predicted relative rotor/backup bearing displacements; top: motor end bearing, bottom: impeller end bearing.
Case2: motor end and impeller ends pinned

Figures 13-15 show predicted behavior for Case 3, rotor shimmed to eliminate clearance in the motor end backup bearing and rotor pinned to the housing on the impeller end. For the simulation, the shimming was modelled by removing the free clearance at the motor end bearing. Figure 13 shows relative rotor/housing displacement at two locations near the motor end. The upper plot is the displacement at the plane of the motor end (brg 1) position sensor. This is shown for comparison to the test data presented in the next section. The peak excursion is close to 0.004 in. The lower plot shows the resilient mount radial displacement which has a peak of about 0.002 in, less than the travel to the hard stop. The relative rotor to backup bearing inner ring travel is insignificant here because of the gap taken up by a shim. Figure 14 shows relative rotor/housing displacement at two locations near the impeller end. The upper plot is the displacement at the plane of the impeller end (brg 2) position sensor. The peak is excursion is close to 0.003 in. The lower plot shows radial displacement of the rotor relative to the impeller end backup bearing. which has a peak of about 0.0025 in so there is no contact with the backup bearing and the margin to contact is better than for Case 2. Figure 15 shows the loads carried by the two backup bearings. The upper plot shows the motor end backup bearing load is well controlled and peaks at about 13 lbf. Because of the shim this bearing will react whatever load is needed to move the rotor along with the housing vibration, but there is no bouncing impact loading. The lower plot confirms no load reacted by the impeller end backup bearing.

The Case 3 locking approach was chosen because it produced good results and appears to be easier to realize reliably in hardware.

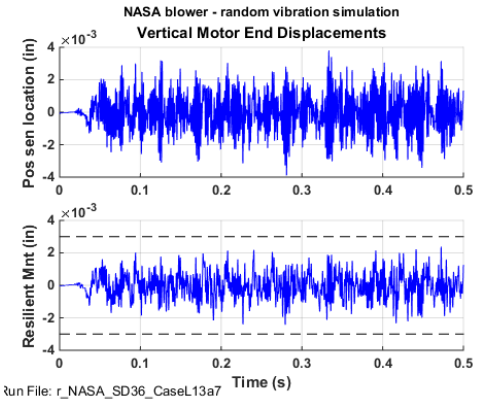

Figure 13. Predicted motor end displacements; top: position sensor location, bottom: across backup bearing resilient mount.
Case3: with motor end shim, impeller end pinned

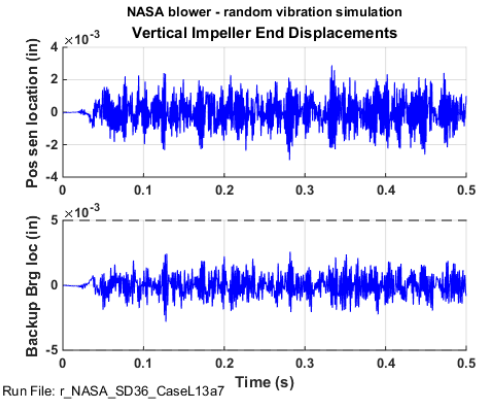

Figure 14. Predicted impeller end displacements; top: position sensor location, bottom: rotor to backup bearing relative displacements.
Case3: with motor end shim, impeller end pinned

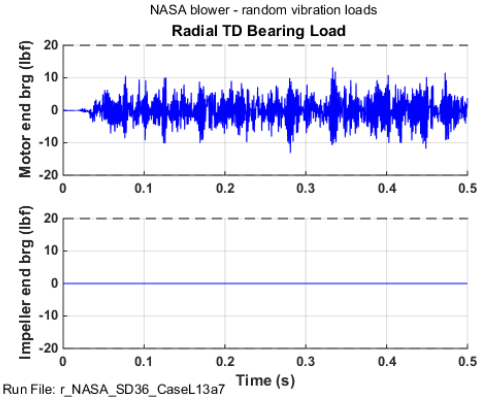

Figure 15. Predicted backup bearing loads: top) motor end; bottom) impeller end.
Case3: with motor end shim, impeller end pinned

Random Vibration Testing

Random vibration testing was performed at a commercial test lab using an electromagnetic shaker. The blower and blower controller were mounted to the shaker which was driven with a time signal that met the PSD requirements in Figure 5. Two control accelerometers mounted on the base plate are part of the shaker feedback loop used to ensure the base motion meets the required profile. The arrangement is shown in the photograph of Figure 16 with the equipment configured for shaking the blower in the horizontal direction. The blower is in the foreground left and the blower controller is in the background right. The rotor locking configuration used is Case 3, motor end backup bearing shimmed, and impeller shaft end pinned, as selected from the analysis. The combined PSD from the two control accelerometers from the vertical testing is shown in Figure 17. The measured PSD was required to be within ±1.5 dB of the specified level from 20 – 500 Hz and within ±3 dB from 500 – 2000 Hz as indicated by the tolerance bands in Figure 17.

Figures 18-21 show relative rotor/housing displacement data taken from the AMB position sensors during the vertical excitation test. Figures 18 (sensor 1) and 19 (sensor 2) show orbit plots for a 10 second period, when the measured peak amplitudes appeared to be at a maximum. The sample frequency of this measurement is 5 kHz. As can be seen in the figures, the direction of response was not purely vertical, as the peak displacements appear to be at a slight angle (approximately 9-15º) relative to the *y*-axis. The maximum peak-peak displacement is about 0.006

in at sensor 1 (motor end) and 0.005 at sensor 2 (impeller end). This can be compared to the simulation results from Figure 14 and 15 of 0.008 in at sensor 1 and 0.006 in at sensor 2. Due to the nature of random vibration, the most definitive outcome of this comparison is that the relationship between the amplitudes from sensors 1 and 2 is similar for the test and prediction. The relatively close correlation in peak amplitudes between this single simulation and the measurement run is encouraging, but repeatability of this correlation was not verified.

Figures 20 and 21 show the corresponding Fast Fourier transforms (FFTs) of the rotor-bearing relative displacement for sensor 1 and sensor 2, respectively. The FFTs are performed over a 2-second period. The FFTs shows the highest response centered around 410 Hz, which should be the lowest resonance of the system. Assuming a rigid connection at the impeller end launch lock and, the model predicted a peak response frequency of approximately 530 Hz for case 3, as noted above. This result seems to indicate that the stiffness contribution from the impeller end launch lock is somewhat lower than modelled. There is also a significant response observed in the primary, vertical axis data in the 20-100 Hz frequency range where the PSD level is 0.35 G2/Hz. This result can also be found in the simulation as well and is due mostly to response at the motor end bearing support. Overall, the test results give confidence in using the model to evaluate the launch locks and in the selection of the locking strategy.

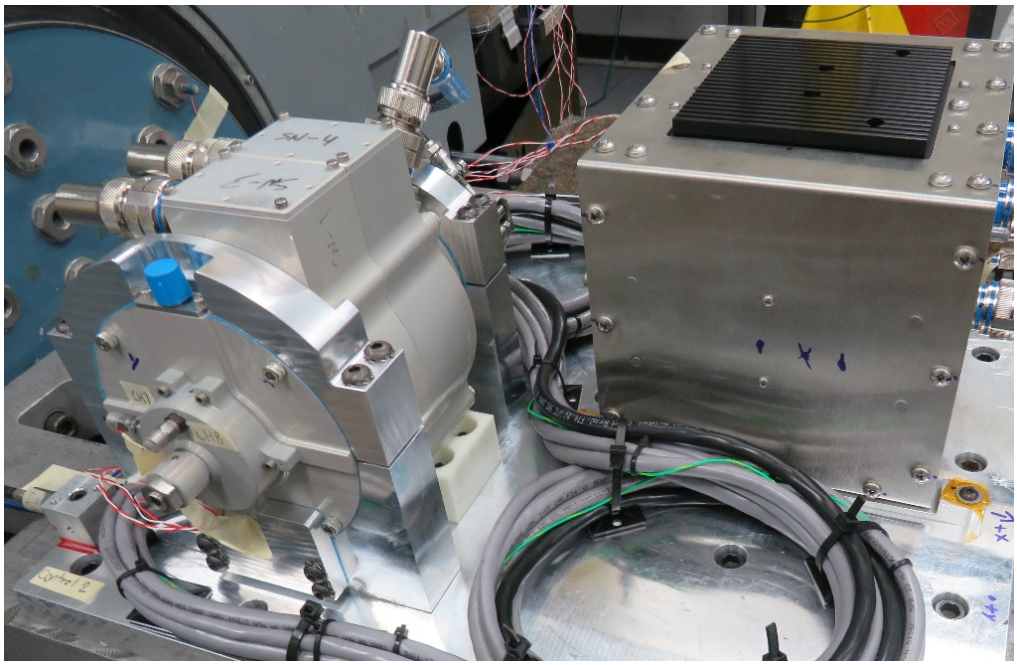

Figure 16. Blower mounted on vibration table prior to random vibration testing. The controller (background) was tested simultaneously on the same base plate.

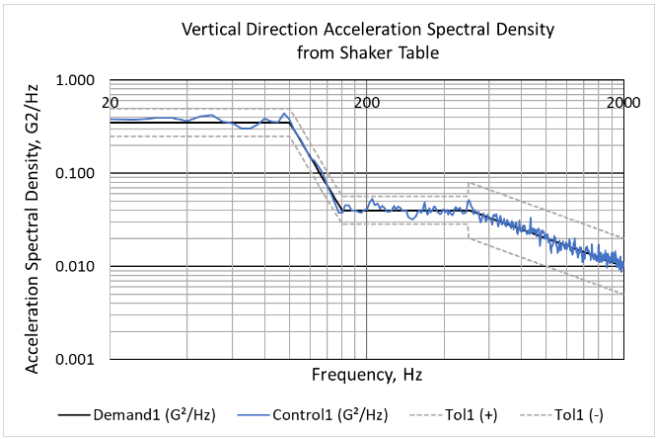

Figure 17. Acceleration spectral density (ASD or PSD) from shaker table control accelerometers, vertical excitation.

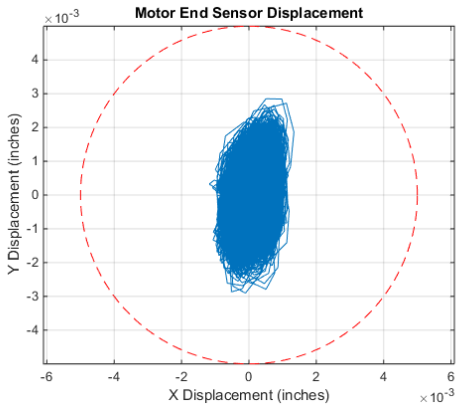

Figure 18. Measured position orbit from motor end AMB sensors (sensor 1) during vertical test.

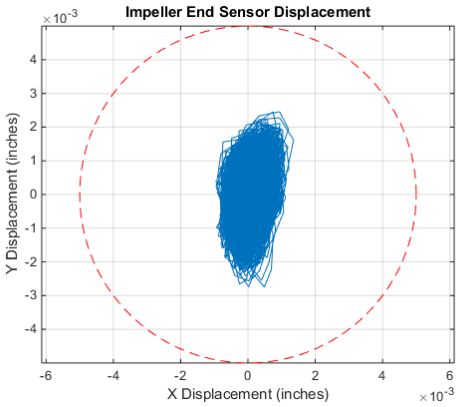

Figure 19. Measured position orbit from impeller end AMB sensors (sensor 2) during vertical test.

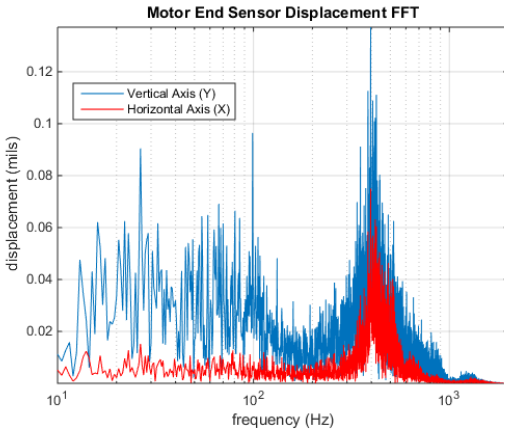

Figure 20. Fourier transform from motor end AMB sensors (sensor 1) during vertical test.

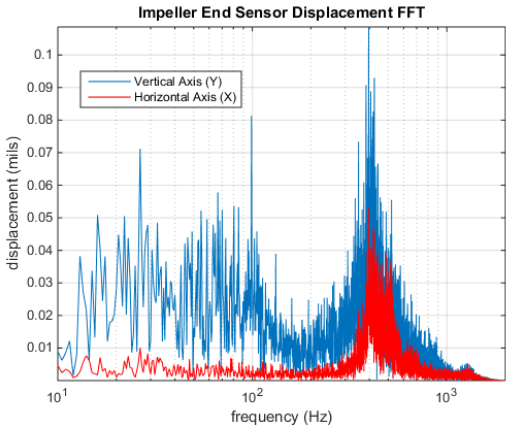

Figure 21. Fourier transform from impeller end AMB sensors (sensor 2) during vertical test.

Conclusion

Random vibration testing has been completed for a magnetically-levitated blower that will be a key component of a new 4BCO2. NASA plans to use the ISS as a test bed to evaluate the scrubber for future space missions. The vibration testing is a standard proof test that NASA imposes to validate that equipment sent to the ISS can survive the launch environment. The vibration testing is considered conservative relative to the launch environment partly because the vibration level imposed during the vibration test is intended to exceed the Maximum Expected Flight Level by 3 dB.

A transient, nonlinear rotordynamic model was developed to simulate the effects of the vibration testing (and subsequently the launch environment) on the blower backup bearings. As the blower will be launched in a de-levitated state, two different methods for locking the rotor were analyzed and compared to a "no launch lock" control case. It was determined that the rotor should be locked to limit rotor motion and backup bearing contact, with an additional shim used to fill the motor-end backup bearing clearance. For the vibration testing, this same locking configuration was used. The results of the vertical shaker test showed that there was 0.006 in. and 0.005 in. peak-peak displacement observed at the motor end sensor and impeller end sensor, respectively. While the simulation predicted somewhat larger amplitudes (0.008 in and 0.006 in), the relationship between the two sensors was the same. Measured results showed a peak displacement at approximately 410 Hz, while the simulation showed a peak response at 530 Hz, likely meaning that the launch lock mechanism was less stiff than modelled.

Overall, the results of the vibration test provide good confidence that the blower can be launched without failure due to random vibration experienced during launch. The simulation results provide confidence that the model can be used for future de-risking of the effect of launch loads on AMB-supported turbomachinery.

References

[1] Hawkins, L., Filatov, A., Khatri, R., DellaCorte, C., Howard, A., 2020, "Design of a Compact Magnetically Levitated Blower for Space Applications", GTP-21-1084, *J. of Eng. For Gas Turbines and Power*, Vol. 143, pp. 091012, September.

[2] API 617 American Petroleum Institute, 2014, *API Standard 617, Eighth Edition, Axial and Centrifugal Compressors and Expander-Compressors*, Washington, D.C., USA, API Publishing Services

[3] Keogh, P., Aeschlimann, B., Hawkins, L., Jayawant, R., Köhler, B., Maslen, E., 2018, "Activities of ISO/TC 108/SC 2/WG 7 in the Development of Standards for AMB Systems", *Proceeding of 16th International Symposium on Magnetic Bearings*, Paper ID-146, Beijing, China, August.

[4] Schweitzer, G., Maslen, E.H, 2009, *Magnetic Bearings: Theory, Design, and Application to Rotating Machinery*, Springer Verlag, Berlin, Germany, pp. 288-294.

[5] Wilkes J., Moore, J., Ransom, D. and Vannini, G., 2013, "An Improved Catcher Bearing Model and Explanation of the Forward Whirl/Whip Phenomenon Observed in Active Magnetic Bearing Transient Drop Experiments," *Proc.of ASME TurboExpo*, GT2013-94594, San Antonio, TX, June.

[6] Smalley, A.J., Darlow, M.S., Mehta, R.K., 1978, "The Dynamic Characteristics of O-Rings", *Trans. Of ASME,* Vol. 100, pp.132-138, January.

[7] NASA, 2015, *Pressurized Payloads Interface Requirements Document International Space Station Program*, SSP-57000 Rev R, October.

[8] Hawkins, L., Wang, Z., Nambiar, K., 2018, "Floating Shock Platform Testing of a Magnetic Bearing Supported Chiller Compressor – Measurements and Simulation Results", *Proc. of ASME Turbo Expo*, GT2018-77031, Oslo, Norway, June.